*Exploration Geophysics (2004) **35**, 70–79*
Butsuri-Tansa (Vol. 57, No. 1)
Mulli-Tamsa (Vol. 7, No. 1)

Application of the tri-axial drill-bit VSP method to drilling for geological survey in civil engineering

Nobukazu Soma[1] Manabu Utagawa[1] Masahiro Seto[2] Hiroshi Asanuma[3]

Key Words: seismic-while-drilling, reflection, downhole measurement, engineering geology

ABSTRACT

We have examined the applicability of the triaxial drill-bit VSP method (TAD-VSP) to the geological survey of possible sites for a high-level radioactive waste disposal repository. The seismic energy generated by a drill bit is measured by a downhole multi-component detector, and the resulting signals are processed to image the geological structure deep underground. In order to apply the TAD-VSP method to civil-engineering-scale drilling, we have developed a small but highly sensitive and precise three-component downhole seismic measurement system, and recorded drill-bit signals at a granite quarry. We have successfully imaged discontinuities in the granite, possibly related to fractures, as highly reflective zones. The discontinuities imaged by the TAD-VSP method correlate well with the results of other borehole observations. In conclusion, the TAD-VSP method is usable in geological investigations for civil engineering because the equipment is compact and it is simple to acquire the drill-bit signal.

INTRODUCTION

We have examined the possibility of using the seismic-while-drilling (SWD) technique as a tool for subsurface imaging, as a part of geological investigations for civil engineering applications. We have studied the technique for the case of development of a high-level radioactive waste disposal repository. With a limited number of exploration boreholes drilled in the initial stage of investigation of the repository, we aim to collect as much geological information as possible from each single exploration hole. Furthermore, it will be possible to evaluate the geological formations adjacent to the repository during development, if we can apply the SWD technique to small-scale drilling activities in the repository galleries. The application of the SWD technique has the potential to add further deep subsurface information at small additional cost.

The SWD technique originated in large-scale drilling activities in the oil and geothermal industries. The seismic signal from a drill bit is used for formation evaluation, for monitoring speed, slipping, and sticking of drill-string rotation, and for reverse Vertical Seismic Profiling (VSP) (Asanuma et al., 1990; Asanuma and Niitsuma, 1995; Rector and Marion, 1991). Reverse VSP by SWD provides the following advantages: (i) real-time information can be acquired during drilling, (ii) observation is simple, easy and compact, (iii) lower costs, because use of an artificial seismic source is not required, and (iv) geological information below the drilling depth can be obtained.

As previous studies of the SWD technique have been mostly for large-scale drilling activity, when compared to drilling in the civil engineering domain, we must initially consider the applicability of the technique to civil engineering applications. During development of a high-level radioactive waste disposal repository, we expect that the SWD technique could be used during a variety of drilling activities, including drilling for geological investigation, core drilling from the surface, construction of the main shaft, excavation of the gallery, small-scale drilling in the gallery for ground water monitoring, and the preparation of holes for radioactive wastes. In such a situation, it is necessary to cope with various different drilling methods, and confined observation conditions such as in the gallery. In the present study, we have looked at the applicability of the SWD technique to small-scale drilling activity. We have considered a case where the length of the borehole is about 500–1000 m, the hole is smaller than 100 mm in diameter, that various drill bits, including coring bits as well as tri-cone bits may be used, and that the geological objective might be either crystalline or sedimentary rock.

The triaxial drill-bit VSP method (TAD-VSP) (Asanuma and Niitsuma, 1995), a type of reverse VSP by SWD, is based on a combination of the drill-bit signal with a downhole multi-component seismic measurement. In this method, we obtain precise 3D particle motion as a 3D hodogram, and image deep subsurface structure by a spatial-temporal correlation analysis. In this analysis we study the 2D problem, but expansion to 3D is straightforward and has been reported by Asanuma et al. (2000) with a 3D polarization analysis. Of the published SWD techniques, the TAD-VSP method is suitable for relatively small-scale drilling in that it uses downhole measurement, which is more advantageous for detecting weak seismic energy than using surface measurement.

In this paper, we introduce the TAD-VSP method for geological investigation in a civil engineering application. Firstly, we briefly explain the TAD-VSP method and show its application using drill-bit signals from a granite quarry. We then describe the characteristics of the observed drill-bit signals, and image the distribution of reflectivities. Finally, these results are interpreted by comparing them with several independent borehole observations.

TRIAXIAL DRILL-BIT VSP METHOD

The TAD-VSP method consists of downhole three-component (3C) seismic measurements at a few points and spatial–temporal cross-correlation analysis based on a coordinate transformation. The configuration of source and detector is similar to reverse VSP.

[1] *National Institute of Advanced Industrial Science and Technology, AIST-west 16-1 Onogawa, Tsukuba 305-8569 JAPAN, Tel: +81 29 861 8254 Fax: +81 29 861 8766 Email: n.soma@aist.go.jp*

[2] *National Institute of Advanced Industrial Science and Technology, Planning Headquarters in Tokyo, 1-3-1 Kasumigaseki Chiyoda-ku, Tokyo 100-8921 JAPAN,*

[3] *Graduate School of Environmental Studies, Tohoku University, Aoba01, Aramaki, Aoba-ku, Sendai 980-8579 JAPAN*

Manuscript received July 4, 2003; accepted September 25, 2003. Part of this paper was presented at the 6th SEGJ International Symposium (2003).

A schematic view of the particle motion vectors in a 2D vertical plane is shown in Figure 1. In the figure, the seismic signals are assumed to propagate as plane waves in an isotropic and low-attenuation medium, which, however, includes scattering points. For simplicity, we also ignore any converted waves, except for a variation of polarization direction. Here, we describe the formulation for the case where both the direct arrival from the drill-bit to the receiver and the reflected arrival are SV-waves. A similar formulation to that which follows is also applicable to the cross-correlation between a direct SV-wave and a reflected P-wave.

Note that the 2D TAD-VSP method cannot use SH-waves in the processing. The spatial–temporal cross-correlation analysis, which is the wave separation process in the TAD-VSP method, cannot separate the direct and reflected arrivals of the SH-waves because their directions of polarization are the same, and are observed by the same component of the receiver.

The particle motion vector of the observed seismic signal $\vec{O}(nT)$ in 2D vertical plane is described by

$$\vec{O}(nT) = \vec{P}(nT) + \vec{SV}(nT - \tau_S) + \sum_{i=1}^{m} k_{Pi}\mathbf{A}_i \vec{P}_{ri}(nT - \tau_{Pi}) + \sum_{i=1}^{m} k_{Si}\mathbf{A}_i \vec{SV}_{ri}(nT - \tau_{Si}), \quad (1)$$

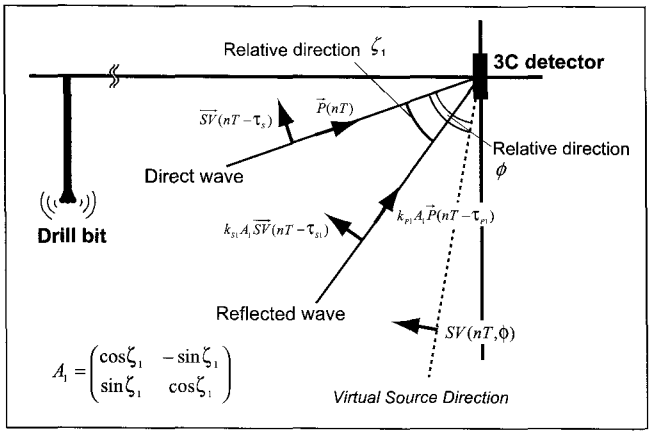

Fig. 1. Particle motion vectors in a vertical plane, and associated terms used in the analysis.

where $\vec{P}(nT)$, $\vec{SV}(nT)$, $\vec{P}_{ri}(nT)$, $\vec{SV}_{ri}(nT)$ are vectors of the particle motion for the direct P- and SV-, and reflected P- and SV-waves, respectively; τ_S, τ_{Pi}, τ_{Si} are delays of the direct SV-wave and the i^{th} reflected P- and SV-waves; k_{Pi}, k_{Si} are reflection coefficients; $\mathbf{A}_i$ is a rotation matrix for the relative direction ζ_i ; n is the sample number; T is the sampling interval; and m is the index number of the reflected wave.

When we assume each reflector (scattering point) acts as a virtual source of waves from the relative direction angle ϕ to the direction of direct arrival, we can make a spatial-temporal cross-correlation analysis of the particle motion to evaluate the relative directions and delays of the reflected waves. For example, the SV-component $SV_v(nT, \phi)$ of the incident wave from virtual source direction ϕ is

$$SV_v(nT,\phi) = P(nT)(-\sin\phi) + SV(nT-\tau_S)\cos\phi + \sum_{i=1}^{m} k_{Pi}P(nT-\tau_{Pi})(-\sin(\phi-\zeta_i)) + \sum_{i=1}^{m} k_{Si}SV(nT-\tau_{Si})\cos(\phi-\zeta_i) \quad (2)$$

where ϕ is the angle of the virtual reflector relative to the direction of direct wave.

Here, the SV-component of the direct arrival from the drill-bit is described as $SV_v(nT, 0)$. We can calculate the 2D cross-correlation function $C_{dv}(\tau, \phi)$ for the delay τ and relative angle ϕ between $SV_v(nT, 0)$ and $SV_v(nT, \phi)$. $C_{dv}(\tau, \phi)$ can be expanded in the following way, if we ignore terms involving the square of the reflection coefficient:

$$\begin{aligned} C_{dv}(\tau,\phi) &= -C_{SP}(\tau+\tau_S)\sin\phi + C_{SS}(\tau)\cos\phi \\ &- \sum_{i=1}^{m} k_{Pi}C_{SP}(\tau+\tau_S-\tau_{Pi})\sin(\phi-\zeta_i) + \sum_{i=1}^{m} k_{Si}C_{SS}(\tau+\tau_S-\tau_{Si})\cos(\phi-\zeta_i) \\ &- \sum_{i=1}^{m} k_{Pi}C_{PP}(\tau+\tau_{Pi})\sin\phi\sin\zeta_i + \sum_{i=1}^{m} k_{Pi}C_{SP}(\tau-\tau_S+\tau_{Pi})\cos\phi\sin\zeta_i \\ &- \sum_{i=1}^{m} k_{Si}C_{SP}(\tau+\tau_{Si})\sin\phi\cos\zeta_i + \sum_{i=1}^{m} k_{Si}C_{SS}(\tau-\tau_S+\tau_{Si})\cos\phi\cos\zeta_i \end{aligned} \quad (3)$$

Here $C_{SP}(\tau)$, $C_{SS}(\tau)$, and $C_{PP}(\tau)$ are the cross-correlation function between SV- and P-waves, the auto-correlation function of SV-waves, and the auto-correlation function of P-waves, respectively, and are given by

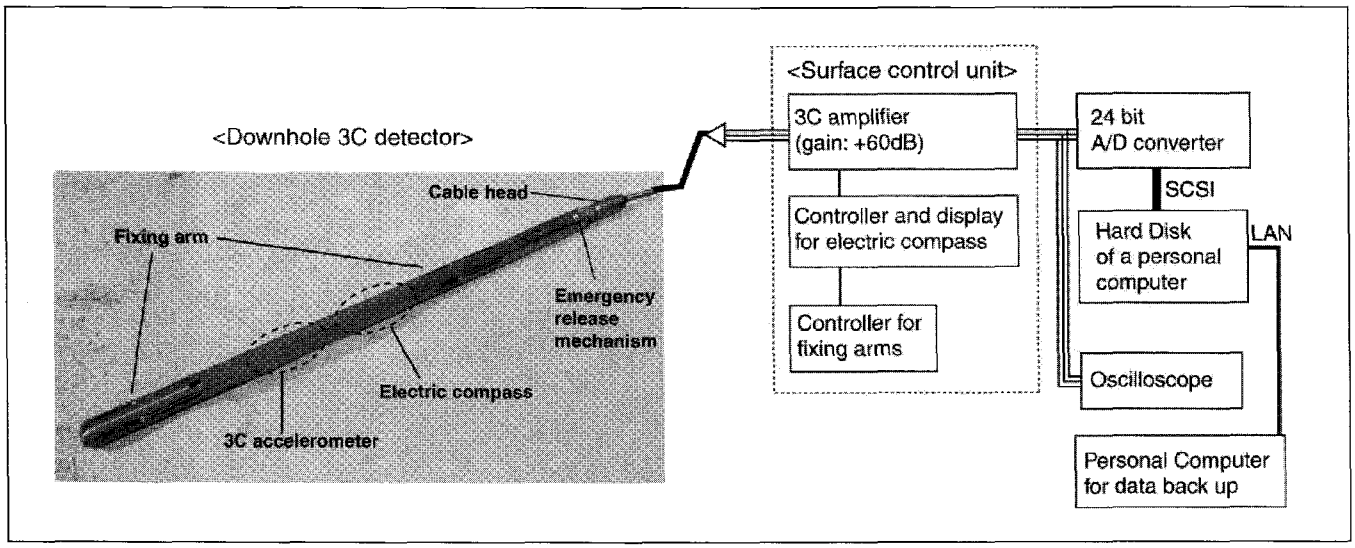

Fig. 2. Overview of 3C seismic detector (left) and block diagram of the measurement system (right).

$$C_{SP}(\tau)=\frac{1}{N}\sum_{i=1}^{N}SV(nT)P(nT-\tau)$$
$$C_{SS}(\tau)=\frac{1}{N}\sum_{i=1}^{N}SV(nT)SV(nT-\tau)\ . \qquad (3a)$$
$$C_{PP}(\tau)=\frac{1}{N}\sum_{i=1}^{N}P(nT)P(nT-\tau)$$

If the spectrum of the recorded signal is broad enough to be regarded as white, we can assume that the auto-correlation functions $C_{SS}(\tau)$ and $C_{PP}(\tau)$ are zero for any $\tau \neq 0$, and the cross-correlation function $C_{SP}(\tau)$ is also zero for any $\tau \neq \tau_S$. Therefore, for $\tau > \tau_s > 0$, equation (3) can be rewritten as

$$C_{dv}(\tau,\phi)=-\sum_{i=1}^{m}k_{Pi}C_{SP}(\tau+\tau_S-\tau_{Pi})\sin(\phi-\zeta_i) + \sum_{i=1}^{m}k_{Si}C_{SS}(\tau+\tau_S-\tau_{Si})\cos(\phi-\zeta_i)\ , \qquad (4)$$

and

$$C_{dv}(0,0)=C_{SS}(0)+\sum_{i=1}^{m}k_{Pi}C_{SP}(\tau_{Pi}-\tau_S)\sin\zeta_i \approx C_{SS}(0)\ . \qquad (5)$$

When the SV-wave energy radiation from a drill-bit can be regarded as uniform in all directions, the second term of equation (4) controls the equation, and gives extrema at the delay of the reflected SV-wave after the direct arrival ($\tau = \tau_{Si} - \tau_S$) and in the propagation direction of the reflected wave ($\phi = \zeta_i$). If the drill-bit source mechanism is assumed to be a single vertical force acting on a free surface, the P-wave is predominantly excited in a vertical direction, and SV-waves propagate horizontally. In this case, most of the energy in the direct wave is SV, and most of the reflected wave energy is P. We can then expect extrema at the delay of the reflected P-wave ($\tau = \tau_{Pi}$) and the propagation direction of the reflected wave ($\phi = \zeta_i$) from a formulation which is similar to equations (1) to (4).

We estimate the reflectivity in this study by normalizing the 2D cross-correlation function with the energy of the SV-component of the direct arrivals:

$$R_{dv}(\tau,\phi)=\left|\frac{C_{dv}(\tau,\phi)}{C_{dv}(0,0)}\right|\ . \qquad (6)$$

Equation (6) describes a ratio between wave energy of direct and reflected waves, which is a kind of reflection coefficient but without any control for effects such as attenuation and radiation pattern.

Practical calculation of the cross-correlation function is performed in the frequency domain using FFT. If the spectra of the drill-bit signals do not have sufficient frequency coverage, or are contaminated by strong periodic noise, the correlation analysis can be strongly affected by periodic artefacts. We employ the generalized cross-correlation technique when the spectrum of the signal is not broad and is not regarded as white (Knapp and Carter, 1976). In the present study, Roth's method is used for the cross-correlation analysis, which is defined as

$$C_{dv}(\tau,\phi)=F^{-1}\left[\frac{S_{SV_0SV_\phi}(f_n)}{S_{SV_0SV_0}(f_n)}\right], \qquad (7)$$

where $S_{SV_\phi SV_\phi}(f_n)$ is the power spectrum of $SV_v(nT, \phi_i)$; $S_{SV_\phi SV_\phi}(f_n)$ is the cross spectrum of $SV_v(nT, \phi_i)$ and $SV_v(nT, \phi_j)$; f_n is the n^{th} frequency component; and F^{-1} denotes the inverse Fourier transform.

By using Roth's method, we can apply the TAD-VSP method to a drill-bit signal that has limited frequency range or is contaminated by periodic noise, although with reduced directional resolution. In equation (7), the term inside the square bracket, $S_{SV_0SV_\phi}(f_n)/S_{SV_0SV_0}(f_n)$, is equivalent to the transfer function between $SV_v(nT,0)$ and $SV_v(nT, \phi_i)$ in a formulation using cross-spectra, and therefore, $C_{dv}(\tau, \phi)$ indicates the impulse response of the transfer function. Hence, the effect of the frequency component of the signal is removed using Roth's method. When ϕ_i equals 0 or 180 degrees, equation (7) is identical with F^{-1}, which means that Roth's 2D cross-correlation loses sensitivity to subsurface structures producing these arrival directions. This phenomenon results from the inapplicability of Roth's method to autocorrelations, as for these directions the direct and reflected components in the cross-correlation agree. This is a theoretical limitation to the use of Roth's method in this situation. Note also that the directional resolution becomes lower when we apply Roth's method.

To image subsurface structure, reflectivities obtained by equation (6) are finally projected onto 2D space assuming a homogeneous velocity.

DOWNHOLE 3C MEASUREMENT SYSTEM

Acquisition of precise 3D particle motion is necessary for analysis by the TAD-VSP method, because accurate coordinate transformations are essential during TAD-VSP processing. Therefore, we require a 3C detector with high sensitivity that can yield precise and accurate measurements of 3D particle motion. We have developed a downhole 3C accelerometer for this purpose (Figure 2). It is composed of three orthogonally mounted sensors, with a sensitivity of 0.31 V/(m/s^2) (or 3.0 V/g), two pairs of fixing arms at the top and bottom of the tool, and an internal direction meter. The noise level of the tool is less than 8×10^{-4} m/s^2. The sensor units are calibrated to have the same phase and sensitivity properties, and the cross-sensitivity between the components is guaranteed to be less than 15%, in order to observe precise 3D particle motion. The detector is 1.45 m long, 60 mm in diameter, and weighs13 kg. The size is smaller than other tools for the same purpose, and this compactness is desirable for surveys in civil engineering fields. For deployment, a short, manually operated 60 m cable is used for shallower surveys. Another 600 m long cable, operated by an electrical winch system, can be used for deeper targets. All components of the measurement system are designed to be compact, and can be handled by a small number of operators; therefore, the system is applicable to field situations where the space for data acquisition is limited. We can measure the drill-bit signal even inside a mining gallery, in situations such as the preparation of drill holes for radioactive wastes in the future operation of a repository.

The signal from the detector is amplified (60 dB gain), and a low-pass filter (f_c = 2 kHz) is applied, in the surface control unit (Figure 2). After amplification and filtering, the signal is sent to a 24-bit A/D converter, and is recorded at a sampling frequency of 5 kHz on the hard disk of a personal computer. The drill-bit signals are recorded into separate files each about one minute long (300 000 samples).

We calibrated the directional sensitivities of each sensor of the 3C measurement system by using a controlled downhole seismic source. We adopted a mechanical type of seismic source, generated by a spring-accelerated weight drop impacter (called

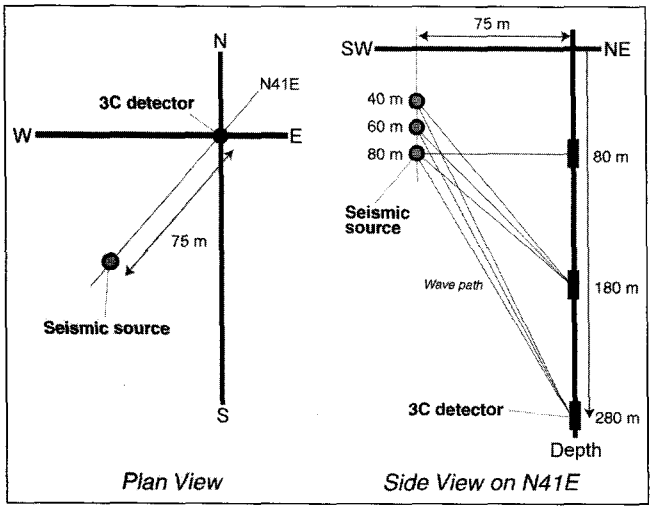

Fig. 3. Schematic diagram of the calibration test layout.

OWS). The distance between source and receiver boreholes was about 75 m. The receiver was located at depths of 80, 180, and 280 m, and the seismic sources were located at 3 depths, of 40, 60, and 80 m. A schematic diagram of the calibration test is shown in Figure 3.

Figure 4 shows the difference between geometrical direction of the source and observed wave direction, plotted against the geometrical inclination of the source from the receiver. The geometrical azimuth was calculated using the position of the two boreholes, and the absolute direction of the x-axis of the receiver defined by internal electric compass, and the geometrical inclination was defined by the position of receiver and seismic source. In the test, the observed arrival directions of shots were calculated by principal component analysis of the 3D hodogram. At the period of the first P-wave arrival, the trajectory of 3C particle motion indicated linear polarization. The averaged differences are 3.3 degrees for inclination and 11.5 degrees for azimuth. The standard deviations are relatively large (around 1 degree for inclination and 2.6–5.6 degrees for azimuth) for incident angles of more that 69 degrees, because the S/N ratio in the data for the

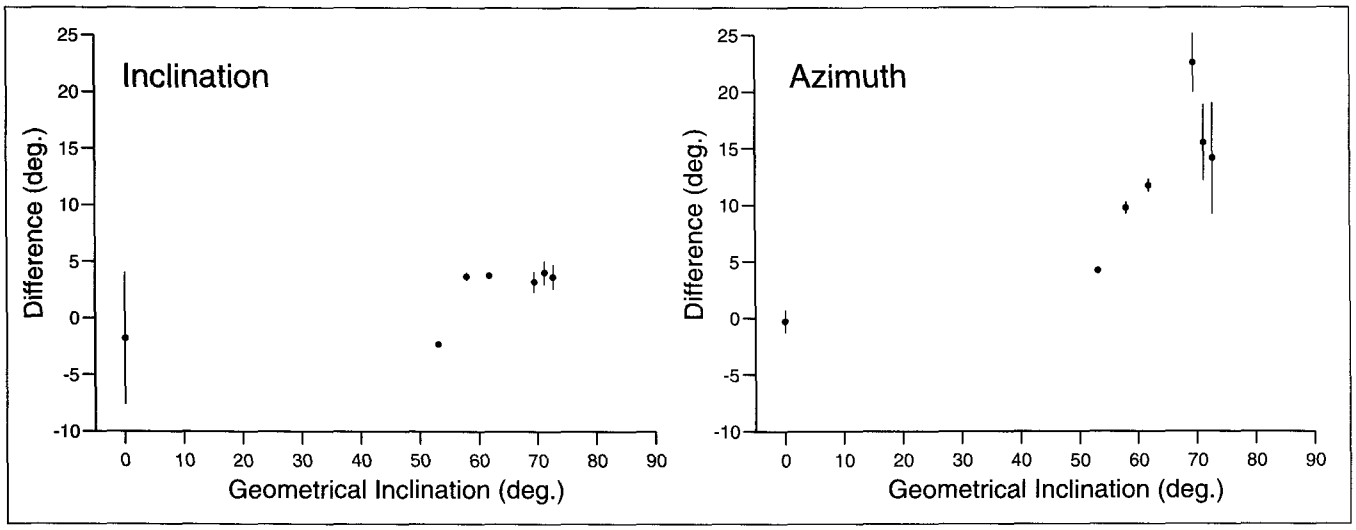

Fig. 4. The result of the calibration test. The differences in inclination (left) and azimuth (right) between geometrical direction of the source and observed wave direction, plotted against the geometrical inclination of source from receiver. The dot and solid bar shows the mean value and standard deviation, respectively from several test shots for each incident angle.

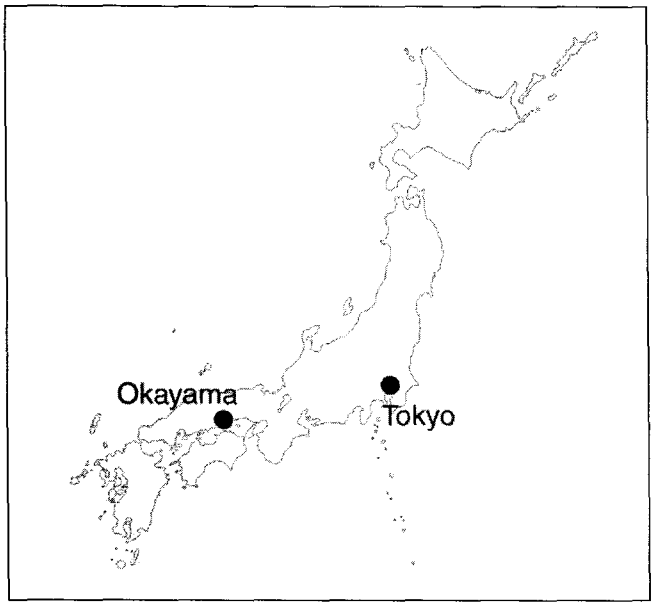

Fig. 5. Location of the test site in Okayama, Japan.

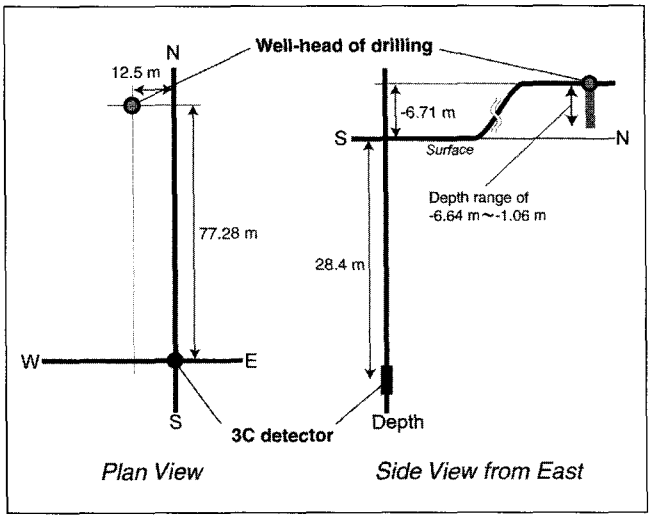

Fig. 6. Layout of the test site, showing the drilling and observation points.

receiver at the deepest depth (280 m) was lower than for other locations. At the incident angle of 0 degrees (that is, with source and receiver at the same level) the calculation of arrival direction was very sensitive to the quality of the recorded first motion of the seismic wave, with the result that the standard deviation in arrival direction is large (5.8 degrees for inclination). Furthermore, the error in azimuth increases for high incident angles, as shown in Figure 4. It is natural that at higher incident angles, the effect of minor differences between the horizontal sensors, such as the noise floor and borehole clamping condition, will be more significant. The error in azimuth is not as serious as that in inclination for the case of 2D analysis in the TAD-VSP method. We consider the differences in detected angle to be small enough at the intermediate incident angles. Therefore, we have concluded the measurement system can receive the seismic signal with sufficient accuracy and has successfully detected the arrival direction of the controlled seismic shots. Thus, the performance of the 3C measurement system is adequate for the analysis in this study.

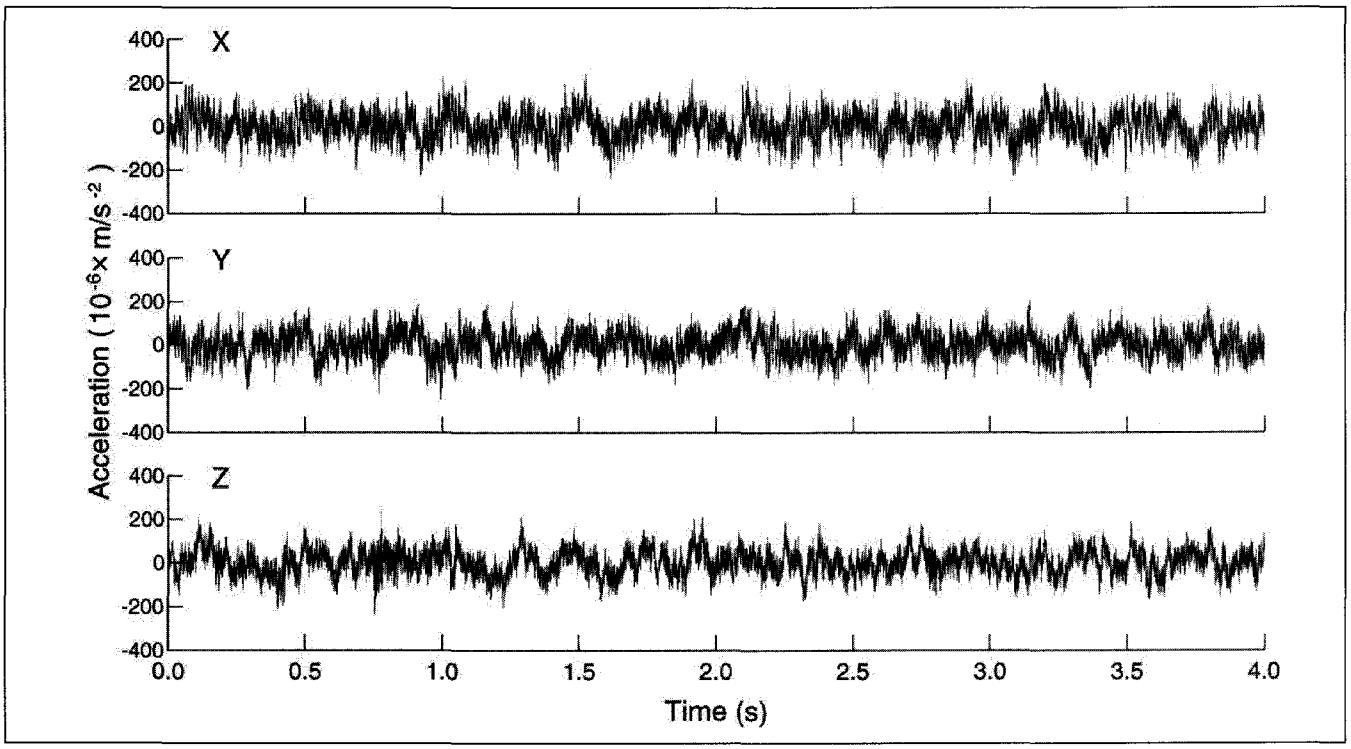

Fig. 7. A four-second example of the observed 3C drill-bit signal.

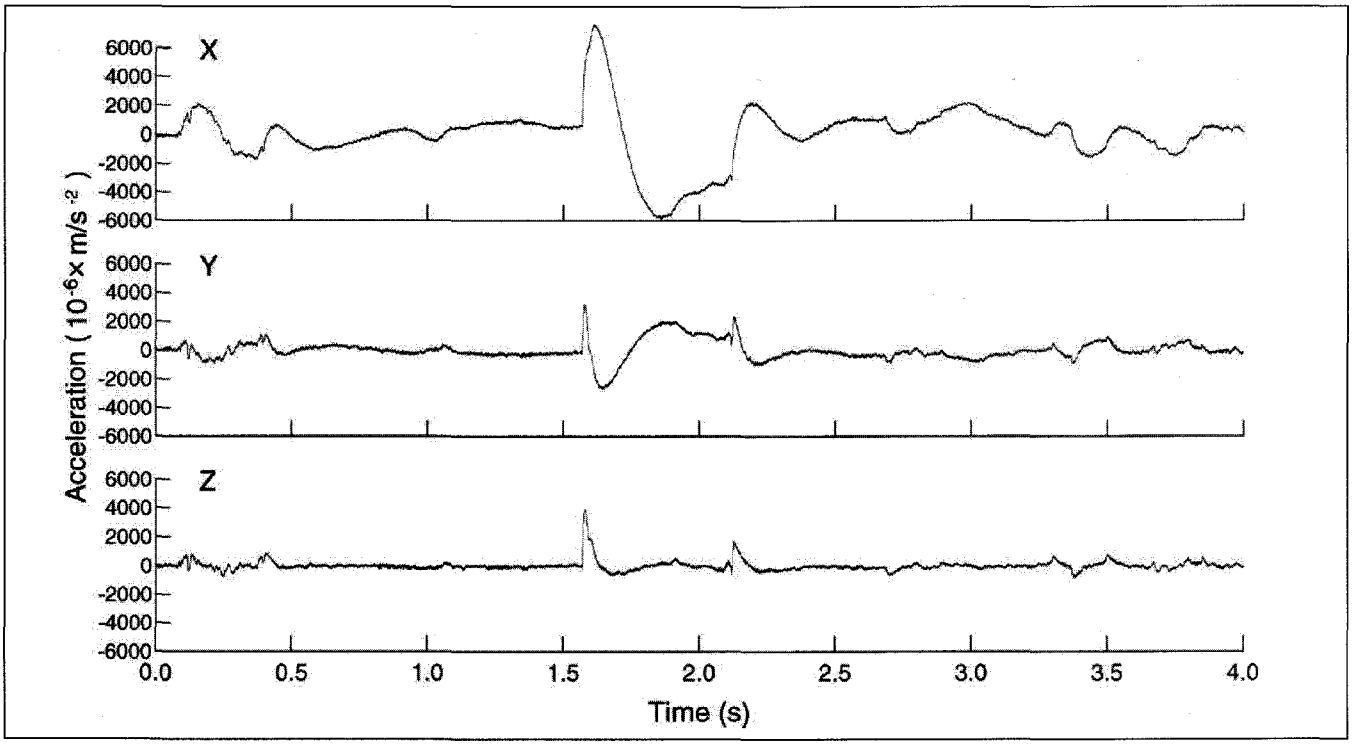

Fig. 8. An example of the 3C drill-bit signal contaminated by strong low-frequency noise.

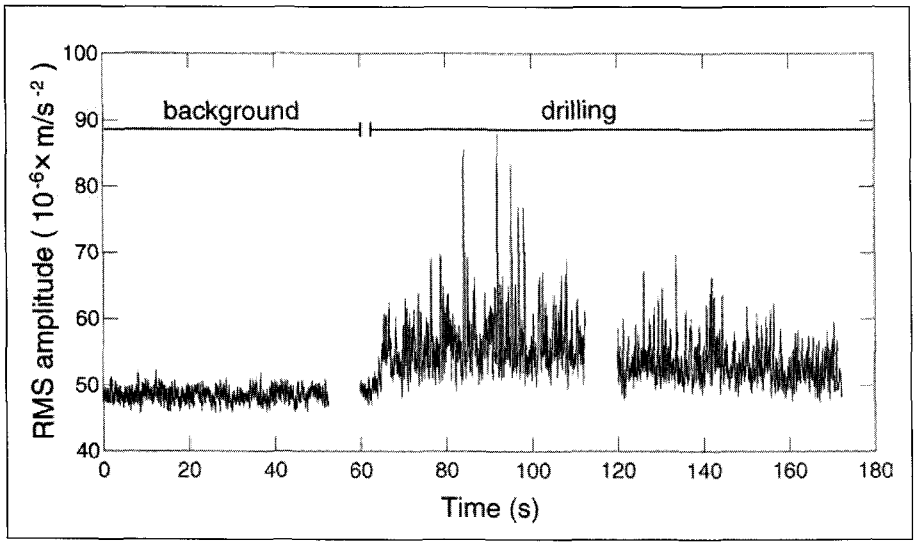

Fig. 9. An example of the RMS amplitude of the drill-bit signal, showing the changes in level as drilling is carried out.

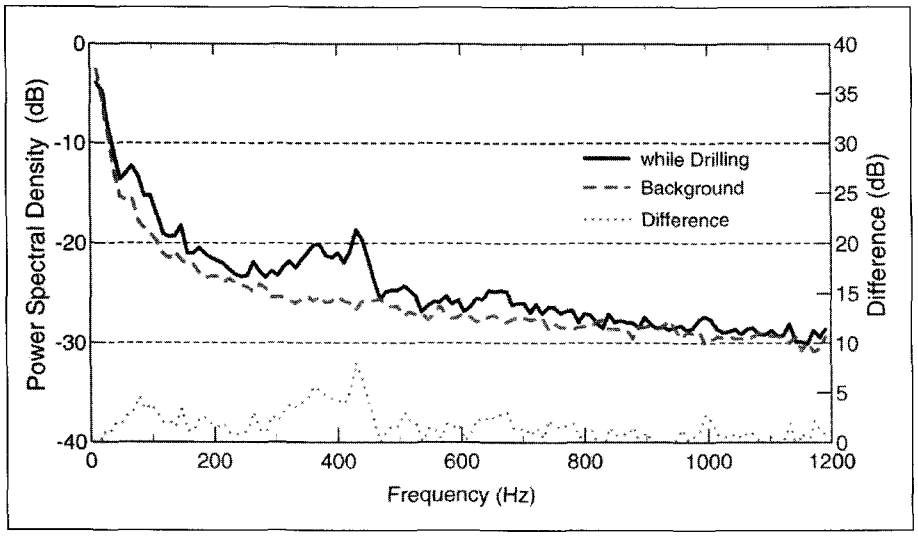

Fig. 10. An example of the mean power spectral density of the drill-bit signal. The black line and the grey broken line are spectra with and without drilling, respectively. The dotted line indicates the difference between these two spectra.

SITE DESCRIPTION AND DATA ACQUISITION

Drill-bit signals were recorded in a granite quarry located in Okayama Prefecture, Japan (Figure 5). We recorded the seismic signal during drilling for in-situ stress measurement, geological investigation, and core sampling. We acquired our measurement only during drilling in the first 10 m, where a tri-cone drill-bit was used. In the first 10 m from the surface (the depth range of -6.71–3.29 m), core drilling was done first with a 96 mm diameter drill bit, and subsequently a tri-cone drill bit, 149 mm in diameter, was used over the same depth interval in order to enlarge the borehole. The weight on the tri-cone drill-bit was about 19600–29400 N, and the rotation speed was about 60 revolutions per minute.

The observation hole was 76 mm in diameter and about 35 m deep. The 3C detector was set at a depth of 28.4 m. The wellhead of the source borehole was 12.5 m west, 77.2 m north, and 6.7 m higher than the wellhead of the observation hole. The maximum distance between the drill bit and the detector was about 86 m. The layout of the observation experiment is shown in Figure 6.

In this study, we have conducted a 2D analysis with the TAD-VSP method, because only one observation point is not enough for estimating 3D subsurface structure. Because the processing of the TAD-VSP method, using Roth's method, is robust for directional differences, it is reasonable to assume a 2D subsurface, unless there is dominant 3D structure.

CHARACTERISTICS OF THE DRILL-BIT SIGNAL

Figure 7 shows examples of drill-bit signals with high S/N ratio, observed by the 3C measurement system. Most data sets were, however, contaminated by strong, very low frequency noise (below 5 Hz), as shown in Figure 8. The noise is thought to be ambient noise possibly caused by traffic, or a nearby factory, because the noise was detected even when all the activity at the quarry was completely stopped.

A change in the root mean square (RMS) amplitude of the 3C signals is an indication that drill-bit signals were probably detected. An example of RMS amplitude variation, at the beginning of tri-cone drilling, is shown in Figure 9. A 0.2 s time window (1000 samples) was used for the calculation of each RMS value. There are three sequences of recorded data, beginning at 15:07, 15:08, and 15:09. In the figure, the RMS amplitude increases at about 63 s, which corresponded to the beginning of drilling.

Figure 10 shows a comparison between the power spectral density of signals observed during drilling, and with no drilling activity (background noise). The power spectral densities were calculated as averaged spectra each totalling 34 minutes of acquired data. From the difference between these two spectra, we see that drill-bit data has broadband coverage from above 50 Hz to about 800 Hz, but that most of the energy is concentrated in the limited frequency range between 300 and 450 Hz. The signal-to-noise ratio around the dominant frequency (430 Hz) is more than 5 dB.

We also displayed 3D hodograms, which are the trajectories of the 3D particle motions, to evaluate the mode of the seismic waves, under the assumption that the main seismic energy is generated by the drill bit. Figure 11 shows a comparison between 3D hodograms with and without drilling. The arrows in the figure show the direction of the drill bit, which basically agrees with the direction of the P-wave arrival. The 3D hodograms after 80 Hz high-pass filtering and coordinate rotation to the SV-SH-P system, assuming the direction of the drill-bit from the detector to be the P-axis, are shown in Figure 12. In the figure, the dominant component of increased wave energy from the drill bit, which we identify from an enlargement of the 3D hodogram, is close to the SV-axis in both the SV-SH and the P-SV planes. Therefore in this paper, we assume that direct arrivals from the drill bit at the receiver are pure SV waves, and we use these in processing with the TAD-VSP method.

ESTIMATION OF SUBSURFACE STRUCTURE BY THE TAD-VSP METHOD

Distribution of the Reflectivities

We applied the TAD-VSP method assuming that the direct wave propagated from the drill-bit to the receiver is an SV-wave. We used relatively good waveforms totalling 34 minutes in recording time. The waveforms were pre-processed with an 80 Hz high-pass filter, to reduce the strong, very low frequency noise shown in Figure 8. In the correlation analysis, Roth's method was applied because the spectrum of the signal was definitely band limited and Roth's method is robust for such spectral deficiencies.

The cross-sections found after applying depth conversion with constant velocities to the results of the TAD-VSP method are shown in Figures 13 and 14. Constant velocities of 4524 m/s for P-wave and 2678 m/s for S-wave were determined by 30 core measurements (Cho, 2001). The results of simple cross-correlation between the direct and reflected arrivals are shown in Figure 13, and those in Figure 14 were processed using Roth's method. In these figures, panel (a) displays the cross-correlation result between the direct SV wave and the reflected SV wave, and panel (b) is the result of cross-correlation between the direct SV wave and the reflected P wave. Assuming P-wave reflection is reasonable when we consider that the P wave is the wave predominantly radiated to the reflector by the directivity of the drill-bit signal. Only the delay range of $\tau > \tau_S$ is considered when performing the cross-correlation between direct SV-wave and reflected P-wave. The images are in the plane that passes through both the drilling and the receiver boreholes. The darker colours in the images correspond to higher reflectivities.

Comparing Figures 13 and 14, it is clear that the limited frequency bandwidth of the drill-bit signal, as shown in Figure 10, causes strong periodic artefacts in the cross-correlation results. On the other hand, judging from the reduction in periodic noise in the results produced using Roth's method, that method works as expected under band-limited conditions.

Directional resolution in this study is severely limited because the spacing between drill-bit and detector is insufficient to detect directional differences effectively. The narrow range of relative direction angle ϕ offers only small differences in the directional weighting defined by the cosine function in equation (4). Moreover, the application of Roth's method leads to the additional reduction of the directional sensitivities of the TAD-VSP method. In the analysis of the direct SV wave and reflected P wave results in Figure 14b, the reflectivity is small for the relative direction of 90 degrees from the direct arrival. Such low reflectivities are to be anticipated by the limitation of Roth's method, in the case of cross-correlation between similar

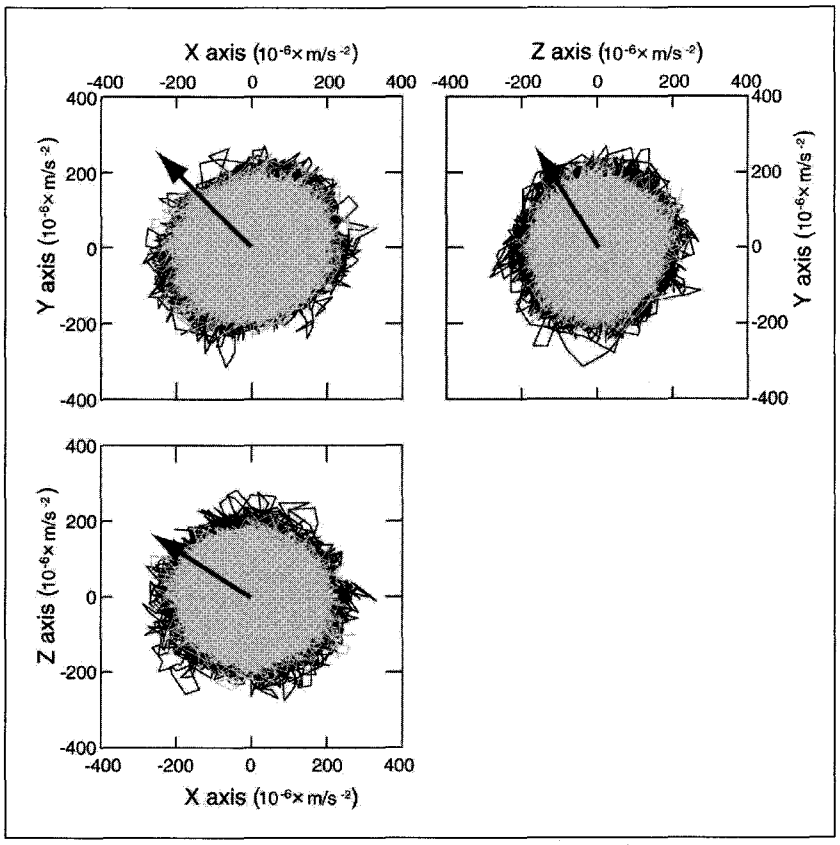

Fig. 11. An example of 3D hodograms of the 3C signal. The black line shows the response when drilling is being carried out, and the grey line is the background noise response. Arrows show the direction of the drill bit.

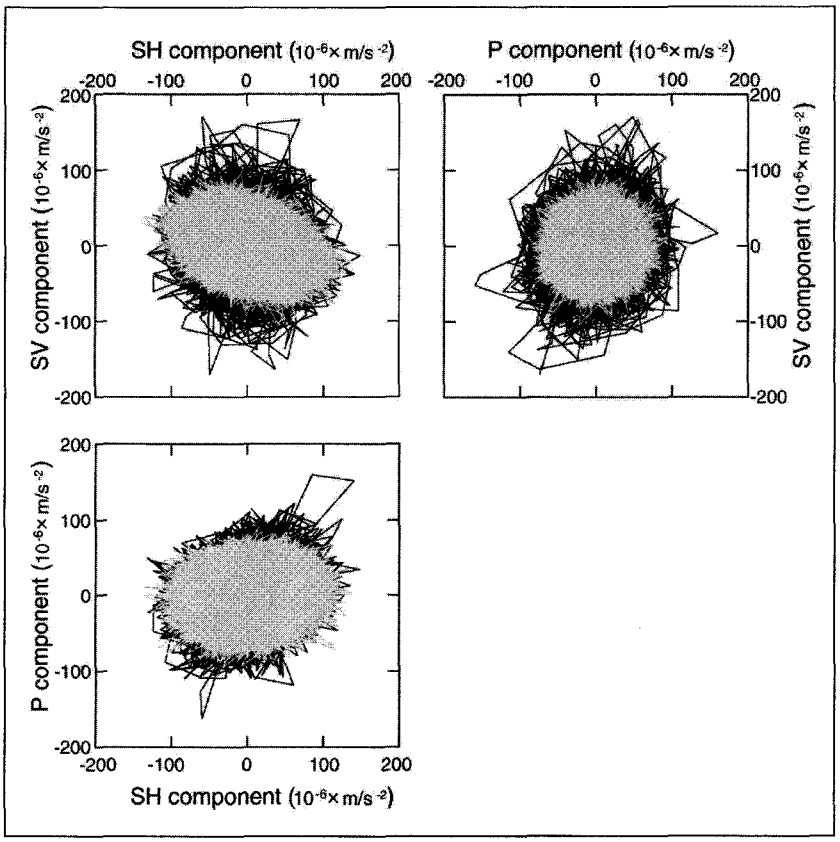

Fig. 12. 3D hodograms of the 3C signal after 80 Hz high-pass filtering, showing motion displayed in the SV-SH-P coordinate system. Black and grey lines show the response with and without drilling, respectively. The drill-bit signals used are the same as those in Figure 9.

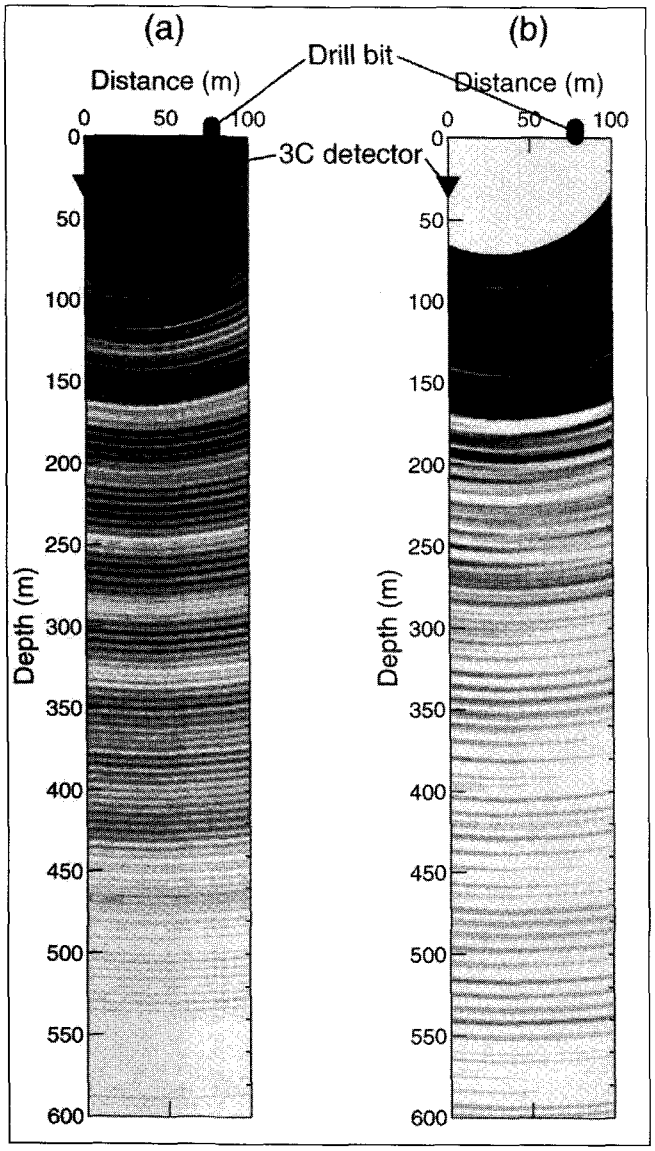

Fig. 13. Reflection images generated by the TAD-VSP method using simple cross-correlation analysis. (a) based on cross-correlation between the direct and the reflected SV wave; (b) based on cross-correlation between the direct SV wave and the reflected P wave. The cross-sections are in the vertical plane through the 3C detector and the drill bit.

components, mentioned in the previous section. As shown in Figure 15, the relative incident angle of the direct SV wave and the reflected P wave is close to 90 degrees, giving rise to the equation (7) identity ($F^{-1}[1]$), and the resulting loss of sensitivity with respect to delay time in Roth's cross-correlation.

Figures 14a and 14b show the subsurface reflectivity images of SV and P waves, respectively. In Figure 14a, highly reflective zones are imaged at depths of 120, 150, and 220 m, and zones of minor reflectivity are also imaged in the figure at depths of 175, 275, 350, 390, 245, and 565 m. Reflective zones can be seen at depths of 200, 240, 260, 300, 355, 390, 425–450, 540–560, and 580 m in Figure 14b. We point out the agreement in depths of zones of high reflectivity imaged in both results at 220–240, 260–275, 350, 390, 425-450 and 560 m. Because of the good agreement between results obtained using different wave modes, the reflective zones imaged by the TAD-VSP method reflect the geological structure with high reliability. Furthermore, it is also possible to conclude that the differences between the images of SV and P wave reflectivity imply characteristics of subsurface structure because of the differing properties of P and SV waves, although artefacts due to unexpected errors in data processing might also be included in these figures.

In the Figure 14, we also compare the results of the TAD-VSP method with a resistivity log (Figure 14c). It seems that most of the observed high reflectivities correspond to anomalies in the resistivity log. The reflectivity anomalies from the TAD-VSP method probably indicate some variations in the granitic rock mass at these depths, and in fact, some fractured zones were detected by both borehole and rock core observations.

Interpretation of the Drill Bit Reflection Image

We have made more precise comparisons between the results of the TAD-VSP method and other well-log results, to a depth of 325 m along the borehole trajectory. Here we only discuss the results that are based on the cross-correlation of direct and reflected SV waves, because the reflectivity determined by direct SV waves and reflected P waves is small along the borehole trajectory, as is shown in Figure 14b. Here we only show results from depths below 75 m, because results of the TAD-VSP method at shallow depth can be strongly affected by the energy in direct waves. The reflectivity imaged by the TAD-VSP method along the drilling borehole is shown in Figure 16a, and well-log results are in Figures 16b–16e. The well-logs include: (b) number of fractures per 2 m, based on BHTV; (c) resistivity; (d) acoustic impedance calculated from density and velocity logs; and (e) a theoretical absolute reflection coefficient for P waves. This reflection coefficient is calculated as $|(a_1-a_2)/(a_1+a_2)|$, where a_1 and a_2 are acoustic impedances averaged over 2 m, calculated from the velocity and density logs, for depths separated by 0.1 m.

The resistivity log shows several peaks around depths of 75, 165, 175, 185, 210, 220, 235, 245, 260, 270, and 325 m. Several small peaks of resistivity are also detected at depth of 75–150 m in short-normal resistivity log. On the other hand, in the results of the TAD-VSP method, high reflectivities appear at depths of 115, 140, 180, 215, 230, 240, and 275 m. These high reflectivities from the TAD-VSP method correspond to depths of both variation in resistivity, and resistivity peaks.

Other logs also show features that can be related to the results from the TAD-VSP method. Peaks in fracture density around the depths of 140, 225, and 275 m correspond to high reflectivities in the TAD-VSP method. Several major peaks of the TAD-VSP method, marked in Figure 16a, correspond to acoustic impedance contrast variations in Figure 16d, such as near depths of 75, 115, 140, 225, and 275 m, although there are small differences in these depths.

We discuss in detail the highest reflectivity anomaly obtained by the TAD-VSP method, at a depth of 215 m. The resistivity log shows a distinct trough at the same depth. Resistivity is often used as an indicator of rock quality, because it is generally sensitive to the existence of water and clay minerals, and so can be highly sensitive to weathering and fracture zones. We conclude that there is a fracture zone around 215 m deep in the rock mass. There is some independent support for our interpretation: firstly, circulation was reported lost during drilling at a depth of 210 m, and secondly, the number of fractures observed by BHTV increases around the depth of 220 m. We then conclude that the TAD-VSP method has successfully identified the fracture zone.

Furthermore, high theoretical absolute reflection coefficients are observed at the same depth as prominent peaks in the result of the TAD-VSP method. This observation supports the reliability of the TAD-VSP method as a tool for subsurface measurement. We

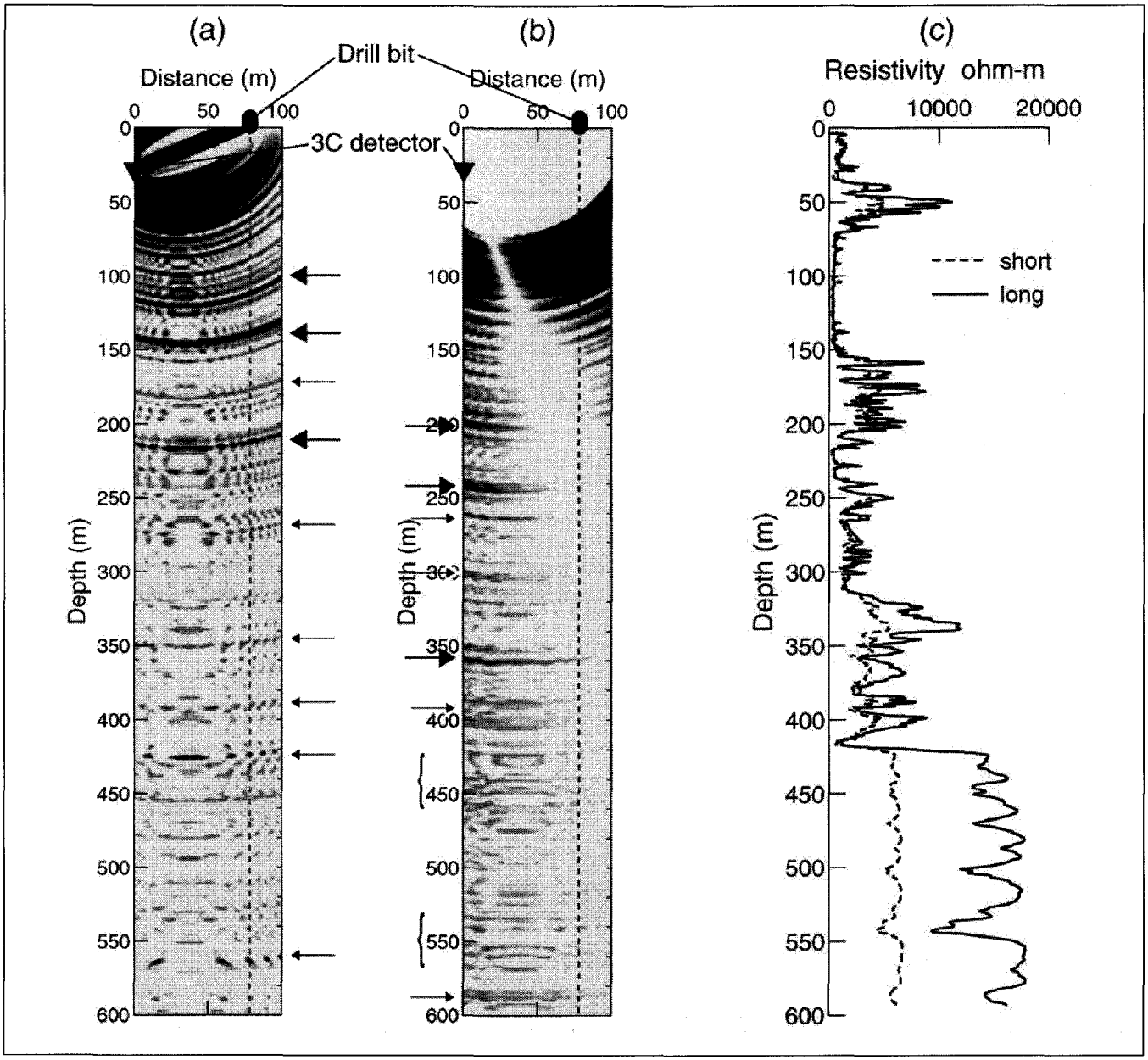

Fig. 14. Reflection images generated by the TAD-VSP method using Roth's method for cross-correlation analysis. (a) based on cross-correlation between the direct and the reflected SV wave; (b) based on cross-correlation between the direct SV wave and the reflected P wave. The resistivity log from the drilled borehole is also shown in panel (c). The cross-sections are in the vertical plane through the 3C detector and the drill bit. The broken line indicates the trajectory of the drilled borehole.

conclude that the TAD-VSP method enables us to image subsurface structure, such as fractured zones in massive granite, to a depth of some hundreds of metres, by simple observation of drill-bit signals while drilling from the surface to depths of 10 m.

CONCLUSIONS

We have examined the possibility of using the TAD-VSP method as a tool for subsurface imaging, as a part of geological investigations in the civil engineering field. We have developed a small-sized downhole 3C seismic measurement system that is applicable to a variety of drilling activities in the civil engineering field. The system allows accurate coordinate transformations, which is essential for the procedures of the TAD-VSP method, because of its high sensitivity and accuracy in measuring particle motion in 3D.

A field test of the TAD-VSP method was carried out at a granite quarry in Okayama, Japan. The drill-bit signals were observed to have spectral coverage from 50 Hz to 800 Hz, with the dominant frequency range around from 300–450 Hz. These band-limited signals resulted in subsurface images with many artefacts.

We imaged the distribution of subsurface P- and SV-wave reflectivities with the TAD-VSP method, and compared the results with several borehole observations, such as the number of fractures observed with BHTV, resistivity logs, and acoustic impedance logs based on density logs and velocity logs. The depths at which high reflectivities were observed coincide with observed variations or peaks in other borehole data. One reflectivity peak was also at a similar depth to an observed fracture zone. The TAD-VSP method in this study has detected variations of rock quality due to weathering or fracture zones inside the granitic rock mass.

We conclude that the TAD-VSP method is usable as an effective technique in geological investigation for civil engineering, as well as in oil and geothermal development, because subsurface images can be created by short-term small-scale drilling. The next step of this project is an examination of the performance of the TAD-VSP method in sedimentary rock, and its application to drilling, such as core drilling, which does not use a tri-cone bit.

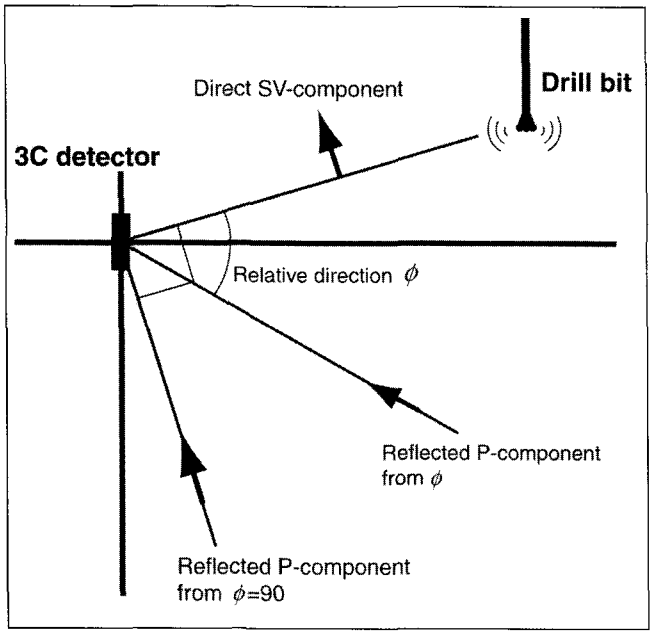

Fig. 15. Schematic relationship between the direct SV component and the reflected P component. Both components are identical when the relative direction angle f is 90 degrees.

ACKNOWLEDGEMENTS

Part of this study was financially supported by the Budget for Nuclear Research of the Ministry of Education, Culture, Sports, Science and Technology, based on screening and counselling by the Atomic Energy Commission. We also thank the Industrial Technology Research Grant Program in 2000 from the New Energy and Industrial Technology Development Organization (NEDO) of Japan for support. We offer our great thanks to Akio Cho for granting permission for, and providing help with, the seismic measurements during drilling, and for providing the borehole data. We thank Toshiyuki Yokota and anonymous reviewers, who contributed to the substantial improvement of this paper.

REFERENCES

Asanuma, H., Liu, H., Niitsuma, H., and Baria, R., 2000, Discrimination of polarization of reflected waves in the triaxial drill-bit VSP and imaging of subsurface structure at Soultz, France: Calgary, Canada: *70th Ann. Internat. Mtg., Soc. Explor. Geophys., Expanded Abstracts.*

Asanuma, H., and Niitsuma, H., 1995, Triaxial seismic measurement while drilling and estimation of subsurface structure: *Geothermal Science and Technology*, **5**, 31–51.

Asanuma, H., Niitsuma, H., and Chubachi, N., 1990, An Analysis of Three Dimensional AE Lissajou Pattern during Well-drilling and Estimation of Source Direction: in Yamaguchi, K., Takahashi, H. and Niitsuma, H., (Eds.), *Progress in Acoustic Emission V: The Japanese Society for Non-Destructive Inspection*, 436–443.

Cho, A., 2001, Report of in-situ rock stress measurement by the hydraulic fracturing method: *Internal document of National Institute of Advanced Industrial Science and Technology.*

Knapp, C.H., and Carter, G.C., 1976, The Generalized Correlation Method for Estimation of Time Delay: *IEEE Trans. Acoustics Speech, Signal Processing*, **24**, 320–327.

Rector III, J.W., and Marion, B.P., 1991, The use of Drill-Bit Energy as a Downhole Seismic Source: *Geophysics*, **56**, 628–634.

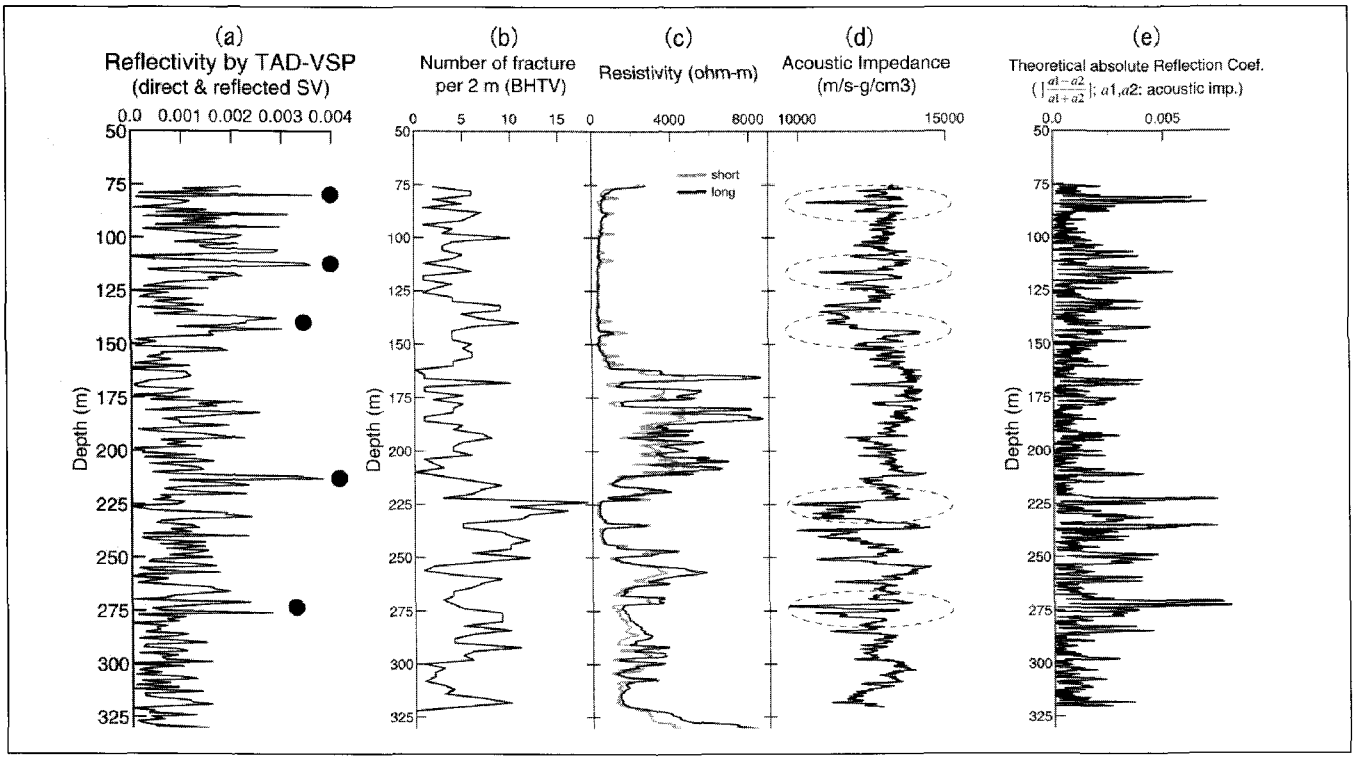

Fig. 16. (a) Distribution of reflectivity along the drilled borehole generated by the TAD-VSP method using cross-correlation between the direct and the reflected SV wave; (b) fracture density log, based on BHTV; (c) resistivity log; (d) acoustic impedance log; (e) theoretical absolute reflection coefficient calculated from the acoustic impedance logs.